

Catalysis Science & Technology

Accepted Manuscript



This is an *Accepted Manuscript*, which has been through the Royal Society of Chemistry peer review process and has been accepted for publication.

Accepted Manuscripts are published online shortly after acceptance, before technical editing, formatting and proof reading. Using this free service, authors can make their results available to the community, in citable form, before we publish the edited article. We will replace this *Accepted Manuscript* with the edited and formatted *Advance Article* as soon as it is available.

You can find more information about *Accepted Manuscripts* in the [Information for Authors](#).

Please note that technical editing may introduce minor changes to the text and/or graphics, which may alter content. The journal's standard [Terms & Conditions](#) and the [Ethical guidelines](#) still apply. In no event shall the Royal Society of Chemistry be held responsible for any errors or omissions in this *Accepted Manuscript* or any consequences arising from the use of any information it contains.

Catalysis Science & Technology

***In-Situ* Fabrication of AgI/AgVO₃ Nanoribbon Composites with Enhanced Visible Photocatalytic Activity for Redox Reactions**

Xiaohan Wang,^a Juan Yang,^{*a} Shuqi Ma,^a Dan Zhao,^a Jun Dai,^b Dafeng Zhang^a

Received xxth xxxxxxxx 20xx, Accepted xxth xxxxxxxx 20xx

DOI: 10.1039/x0xx00000x

www.rsc.org/

Abstract: AgI/AgVO₃ nanocomposites have been newly synthesized through a facile in-situ ion exchange approach with β -AgVO₃ nanoribbons as Ag source and support to immobilize AgI. The as-prepared composites can be served as high-efficient visible-light-driven photocatalysts toward selective oxidation of benzylic amine into imine and reduction of toxic ions Cr(VI). It is found that the mole ratios of AgI have an essential effect on the photocatalytic redox activity and the highest photocatalytic performance is obtained over 20% AgI/AgVO₃ nanocomposite. In-situ growing AgI on the surface of β -AgVO₃ nanoribbons facilitates the formation of close interfacial contact, which thus improves the separation of photoinduced electron-hole pairs. On the basis of detailed characterizations of typical sample 20% AgI/AgVO₃ before and after photocatalytic reactions, Ag⁰ species is formed in the initial stage of reactions. The considerable improvement of photocatalytic redox properties of AgI/AgVO₃ is mainly ascribed to the efficient separation of photoinduced electrons/holes via a Z-scheme bridge mechanism of formed Ag/AgI/AgVO₃, in which Ag nanoparticles serve as the charge migration bridge.

Keywords: AgI/AgVO₃, visible-light-driven, redox ability, ion exchange, Z-scheme mechanism

1. Introduction

The trapping and converting of solar energy over semiconductors and the resulting heterogeneous photocatalysis have attracted ever-increasing attention owing to the potential as one of most promising and green method to solve the present energy and environment problems.¹⁻³ Among various semiconductor-based photocatalysts, TiO₂ has proven to be a superior candidate especially for the photocatalytic degradation of contaminations and splitting of water to H₂, because of its excellent reactivity and stability.⁴⁻⁶ However, TiO₂ shows limited quantum yields owing to low separation efficiency of photoinduced electrons/holes and lacks visible-light response because of large band gap of 3.2 eV. Hence, the studies on constructing high-efficiency photocatalysts with visible-light response are becoming the focal issues in the field of photocatalysis.

In recent years, Ag-based compounds have been recognized as novel visible-light driven photocatalysts on photocatalytic degradation of pollutants or splitting water into O₂, such as Ag₃PO₄,⁷⁻⁹ AgX (X = Cl or Br),^{10,11} and Ag₂CO₃.^{12,13} Whereas, there are several intrinsic factors in restricting their practical applications under visible-light irradiation. For example, the above-mentioned Ag-based materials are usually unstable and the unavoidable decomposition generally gives rise to Ag particles on the surface of photocatalysts during the photocatalytic process. Besides, more positive conduction band potential of these Ag-based photocatalysts restricts their utilizations in photocatalytic reduction reactions. As a result, further researches are necessary to improve the activity and stability of Ag-based photocatalysts.

Among these Ag-based compounds, β -AgVO₃ has recently gained widespread attention because of their excellent properties in rechargeable lithium batteries, bacterial inactivation and H₂S sensors.¹⁴⁻¹⁶ Additionally, the unique hybridization of valence bands of V 3d, O 2p, and Ag 4d orbitals in AgVO₃ gives rise to a narrow band gap and highly dispersed valence band, which can be served as visible-light-driven photocatalyst.¹⁷⁻¹⁹ Meanwhile, β -AgVO₃ shows relatively high stability to photo or chemical corrosion than the other Ag-based materials. However, the photocatalytic performance of β -AgVO₃ is limited, which might be attributed to the low separation efficiency of photogenerated charge carriers. Thus, the studies on improving the separation of photoinduced electrons/holes are extremely important to promote the photocatalytic activity of β -AgVO₃. Generally, the fabrication of a

photocatalyst with specific morphology is considered as one of most effective methods to improve the catalytic performance. Among the different architectures of silver vanadate, one-dimensional nanoribbons have gained considerable interest in photocatalytic field because of their large aspect-ratio and the resulting effective charge separation.^{15,18,19}

Furthermore, photocatalytic activity of a catalyst is greatly dependent on the separation efficiency of photogenerated charge carriers. Construction of hetero-structure or nanocomposite with the other materials having appropriate energy band is proved to be an effective way to improve the separation of photoinduced electron-hole pairs and photocatalytic property of β -AgVO₃. Very recently, Geng et al. demonstrated that AgVO₃@AgBr@Ag nanobelt heterostructures displayed superior photocatalytic performance over bare β -AgVO₃ for removing organic dye rhodamin B (RhB) under the irradiation of visible light.²⁰ Liao and co-workers reported that the obtained one-dimension Ag/AgVO₃ photocatalysts showed high activity for photocatalytic degradation of dye pollutants basic fuchsin (BF) and crystal violet (CV).^{21,22} Additionally, BiVO₄@ β -AgVO₃ nanocomposites were synthesized through an in situ growth process, which exhibited enhanced photocatalytic property compared to single AgVO₃ and BiVO₄.²³ However, the photocatalytic researches of AgVO₃-based composites have primarily focused on traditional “nonselective” photocatalytic oxidative degradation. To the best of our knowledge, application of AgVO₃ hybrid materials as visible light-driven photocatalysts for selective photocatalytic oxidation remains underreported so far. In particular, compared to photocatalytic oxidation processes, photocatalytic reduction reactions are less studied over AgVO₃-based composites, owing to their positive conduction band potential and the resulting weak reductive properties.

In this study, to enhance the photocatalytic redox property of β -AgVO₃, AgI having matched energy band levels is selected as a proper component to couple with AgVO₃. AgI/AgVO₃ composites with different mole ratios are newly synthesized through an in-situ ion-exchange approach, as utilizing β -AgVO₃ nanoribbons as Ag source. Facile in-situ growth strategy can effectively restrain the aggregation of AgI and facilitate the formation of intimate interfacial contact between AgI and β -AgVO₃. The as-prepared AgI/AgVO₃ nanoribbon composites exhibit much higher photocatalytic redox activity than single AgI or AgVO₃ toward selective oxidation of benzylamine into imine and

reduction of toxic ions Cr(VI) under visible light illumination. The considerable improvement of photocatalytic redox properties of AgI/AgVO₃ is mainly ascribed to the efficient separation of photoinduced electrons/holes and more negative conduction band potential of coupled AgI. Based on the characterization of catalysts before and after photocatalytic reactions and the formation of superoxide radicals, possible photocatalytic mechanism of highly improved redox activity over AgI/AgVO₃ nanoribbon composites is also elucidated.

2. Experimental

2.1 Preparation of AgI/AgVO₃ nanoribbon composites

In a typical process, 0.117 g of ammonium vanadate was dissolved in 60 mL deionized water under stirring to obtain a transparent solution. Then, 0.167 g of silver nitrate was added into the above solution and stirred for 5 min. The pH value of the solution was adjusted to 8-8.2 by using NH₃·H₂O (25-28%) and the mixture was transferred into a 100 mL autoclave with a PTEE container inside, which was maintained at a hydrothermal temperature of 180 °C for 12 h. The precipitate was collected after filtering, washed with deionized water and dried at 70 °C for 10 h to obtain AgVO₃ nanoribbons.

AgI/AgVO₃ nanoribbon composites were synthesized via a facile in-situ ion-exchange approach. 0.5 g of AgVO₃ was added into 100 mL of deionized water, which was sonicated for 30 min. A certain amount of potassium iodide was dissolved in 30 mL of deionized water to prepare KI aqueous solution. The obtained KI solution was dropped into the above AgVO₃ suspension, which was then stirred for 5 h at room temperature. After that, the final precipitates were recovered, washed with water, and dried at 60 °C for 12 h. According to the method, different AgI/AgVO₃ nanoribbon composites with I/V molar ratios at 5%, 10%, 20%, 30%, and 40% were prepared and denoted as 5% AgI/AgVO₃, 10% AgI/AgVO₃, 20% AgI/AgVO₃, 30% AgI/AgVO₃, and 40% AgI/AgVO₃, respectively. For comparison, bare AgI was prepared by mixing KI solution with AgNO₃ solution in NH₃·H₂O.²⁴

2.2 Catalyst characterization

Crystalline structures of the samples were identified by using a D8 Advance X-ray diffractometer (Bruker) with Cu K α radiation ($\lambda = 0.15405$ nm) in the range of 5-80° (2 θ). The images of

micro-morphology were observed by scanning electron microscopy (SEM, Hitachi, S4800). Energy-dispersive X-ray (EDX) spectroscopy being attached to SEM was used to measure chemical composition of samples. BET surface area of AgI/AgVO₃ composites was recorded by using Autosorb iQ surface area analyzer and AsiQwin software. XPS measurements were performed on a Thermo Scientific ECALAB 250xi system with Mg K α source. All the binding energies were calibrated by C_{1s} peak at 284.8 eV of surface adventitious carbon. Ultraviolet-visible diffuse reflectance spectra (UV-vis DRS) were recorded using a UV-vis spectrophotometer (UV-2550, Shimadzu, Japan) using BaSO₄ as reflectance standard. Photoluminescence spectra (PL) of the catalysts were recorded using a PerkinElmer LS55 Fluorescence Spectrophotometer with a 400 nm excitation wavelength. Electron spin resonance (ESR) signals of the radicals spin-trapped with 5,5-dimethyl-1-pyrroline-N-oxide (DMPO) were recorded on a Bruker ER200-SRC spectrometer at ambient temperature, using the settings: 20 mW microwave power, 100 G scan range and 1 G field modulation. The photoinduced current density were carried out in a three-electrode system and the working electrode was prepared according to the previous report.²⁵ Platinum foil and saturated calomel electrode served as the counter electrode and reference electrode. The measurements were performed on a CHI Electrochemical Workstation (CHI 760D, Shanghai, China) and the electrolyte was 0.5 mol·L⁻¹ Na₂SO₄ aqueous solution (pH ~ 6.8).

2.3 Photocatalytic activities

Light source for photocatalytic reactions is a 300 W Xe lamp (PLS-SXE 300, Beijing Perfect Light Co., Ltd.) with 400 nm cutoff filter. Photocatalytic selective oxidation of benzylamine was carried out in a 25 mL round-bottomed Pyrex glass flask equipped with a sealed spigot. Typically, benzylamine (0.25 mmol) and catalyst (50 mg) were dispersed into the solvent of acetonitrile (10 mL). Prior to the irradiation, the mixture was stirred for 0.5 h in dark to ensure the formation of homogeneous suspension. After the reaction, about 1.5 mL of mixture was collected and filtered by using a Millipore filter (pore size 0.45 μ m) to completely remove the catalyst particles. The remaining filtrate was quantitatively analyzed on an Agilent 7890 gas chromatography (GC) equipped with a standard FID detector and a DM-5 amine capillary column (30 m \times 0.5 mm \times 0.25 mm, Dikma) using highly pure N₂

as the carrier gas. Standard analytical conditions: injector temperature 230 °C, FID detector temperature 300 °C, column temperature program: 40 °C (hold 6 min) to 280 °C (hold 4 min) at 25 °C·min⁻¹. Benzylamine and the derivatives were determined by comparison of retention times with authentic samples. The structures of products were confirmed by comparison of the retention times with standard samples and further confirmed by gas chromatography-mass spectrometry (GC-MS). GC-MS (Thermo-Finingan Trace 2000/Trace DSQ) analyses were carried out with a GsBP-5MS capillary column (30 m × 0.25 mm × 0.25 μm, Dikma) and high pure He as the carrier gas with a same temperature program as that of GC.

Controlled photoactivity experiments using different radical scavengers (triethanolamine^{26,27} as the scavenger for photogenerated holes, tetrachloromethane²⁸ as the scavenger for electrons and benzoquinone²⁹ as the scavenger for superoxide radical species) were carried out through the similar process to the above photocatalytic oxidation of benzylamine except that the radical scavengers (0.2 mmol) were added to the reaction system.

As to the photocatalytic reduction of Cr(VI), 50 mg photocatalyst was dispersed into 50 mL Cr(VI) solution (20 mg·L⁻¹), based on Cr in a dilute K₂Cr₂O₇ solution. The obtained suspension was stirred in dark for 30 min to ensure adsorption-desorption equilibrium before the irradiation with 300 W Xe lamp. During the photocatalytic reduction of Cr(VI), 3 mL of reaction solution was taken out at a certain interval and centrifuged to remove the catalyst particles. The residual amount of Cr(VI) in the solution was analyzed on the basis of its characteristic optical absorption at ca. 371 nm, using a Cary 100 UV-vis spectrophotometer (Varian Co.) to measure the change of Cr(VI) concentration with irradiation time based on Lambert-Beer's law. The percentage of Cr(VI) removal is indicated as $(C_0 - C)/C_0$. Here, C is the characteristic absorption of Cr(VI) solution at each irradiation time interval, and C_0 is the absorption of the initial solution prior to irradiation.

3. Results and discussion

3.1 Catalyst characterization

Fig. 1 displays the XRD patterns of as-prepared β-AgVO₃ nanoribbons, AgI and AgI/AgVO₃ composites

with different amounts of AgI. The diffraction peaks of pure β -AgVO₃ sample (Fig. 1a) match well with those of standard monoclinic phase (JCPDS 29-1154).²⁰⁻²³ The XRD patterns of the prepared AgI (Fig. 1g) coincide with the hexagonal β -AgI phase (JCPDS 85-0801).^{30,31} It can be clearly observed (Fig. 1b-f) that all the AgI/AgVO₃ composites display a coexistence of both AgI and AgVO₃ phases. For the as-prepared composites, the diffraction peaks intensity of AgI becomes stronger with increasing of AgI amounts. Additionally, the diffraction peak positions of β -AgVO₃ do not shift, which suggests that compounding of AgI does not influence the crystal structure of β -AgVO₃.

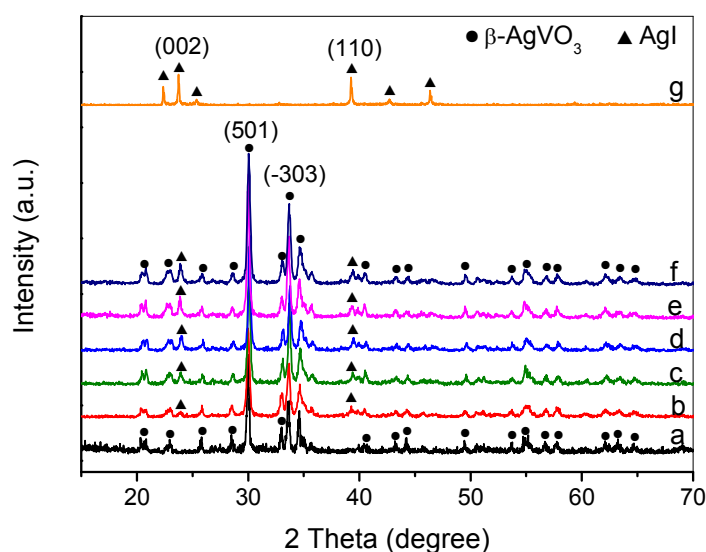


Fig. 1 XRD patterns of β -AgVO₃ nanoribbons (a), 5% AgI/AgVO₃ (b), 10% AgI/AgVO₃ (c), 20% AgI/AgVO₃ (d), 30% AgI/AgVO₃ (e), 40% AgI/AgVO₃ (f), and AgI (g).

The morphologies of as-prepared bare β -AgVO₃ and AgI/AgVO₃ composites are characterized by using SEM and the images are given in Fig. 2. It is observed from Fig. 2a that bare β -AgVO₃ consists of ultralong nanoribbons with a length of several tens of micrometers. Through in-situ ion-exchange between AgVO₃ and KI, small AgI nanoparticles (the bright spots in Fig. 2b-f) are anchored on the surface of β -AgVO₃ nanoribbons, whereas the ribbon-like morphology of bare AgVO₃ remains unvaried for the as-obtained AgI/AgVO₃ composites via the ion-exchange reactions. Furthermore, it can be found that the distribution and size of AgI particles are greatly dependent upon the mole ratios

of KI to AgVO_3 . When the ratio of KI to AgVO_3 is 5 %, several AgI nanoparticles (about 60 nm, Fig. 2b) are formed on the surface of AgVO_3 nanoribbons. With an increase in the mole ratios of KI/ AgVO_3 , more AgI particles are observed on the nanoribbons and the size of AgI becomes larger. As the mole ratio of KI/ AgVO_3 increases up to 40%, the formed AgI has a size of about 200-400 nm (Fig. 2f). The amount and size of in-situ formed AgI nanoparticles upon $\beta\text{-AgVO}_3$ nanoribbon increase with the molar ratio of KI to AgVO_3 , which coincides with the XRD results in Fig. 1. Besides, blank AgI prepared by mixing KI with AgNO_3 solution in $\text{NH}_3\cdot\text{H}_2\text{O}$,²⁴ displays irregular particles (about 200-500 nm) and their aggregates (2-3 μm) (Fig. S1, ESI[†]). Hence, in-situ ion-exchange method can inhibit the aggregation of AgI and benefit to formation of homogeneous nanoparticles.

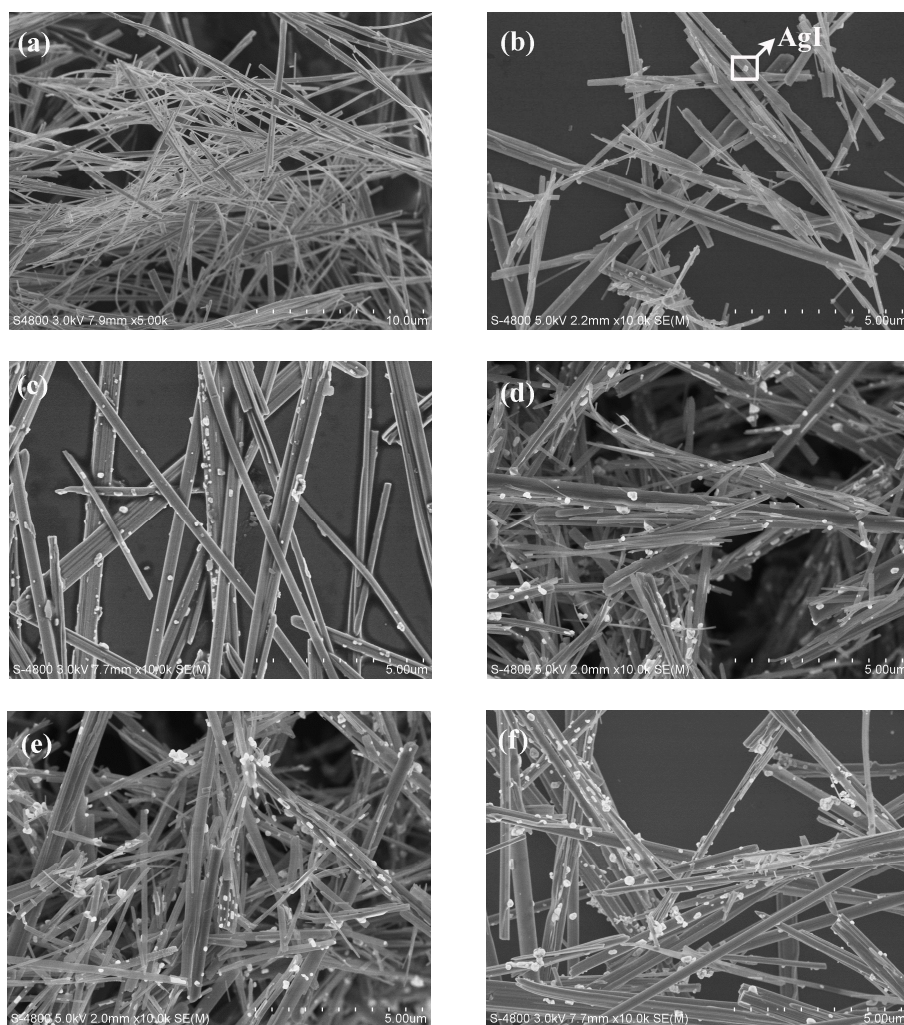


Fig. 2 SEM images of $\beta\text{-AgVO}_3$ nanoribbons (a), 5% AgI/ AgVO_3 (b), 10% AgI/ AgVO_3 (c), 20%

AgI/AgVO₃ (d), 30% AgI/AgVO₃ (e), and 40% AgI/AgVO₃ (f).

The structure of the composite 20% AgI/AgVO₃ is further investigated by TEM and HRTEM. Fig. 3a indicates that some nanoparticles are deposited upon the surface of β -AgVO₃ nanoribbons. The HRTEM image of the magnified view of the red-square area is given in Fig. 3b. As can be seen, two sets of different lattice fringes can be observed. The lattice fringe of 0.777 nm corresponds to the (-101) crystal plane of β -AgVO₃²³, whereas the lattice fringe of 0.273 nm matches well with the (102) plane of β -AgI.³² These results further confirm the formation of AgI/AgVO₃ heterostructures, thereby improving the charge transfer between them.

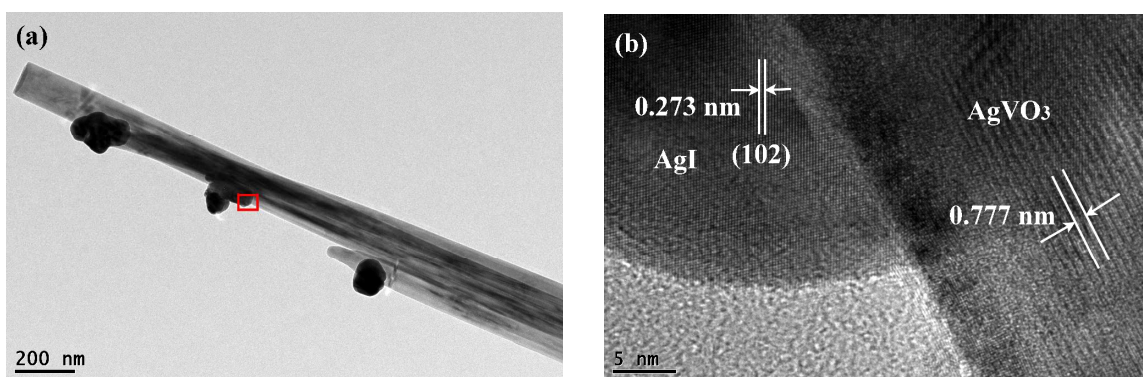


Fig. 3 (a) TEM image of 20% AgI/AgVO₃ composite, (b) HRTEM image of the designated square area in panel (a).

The sample's composition and surface area are also measured and summarized in Table 1. Pristine AgVO₃ sample consists of Ag, V, and O elements and the Ag/V atom ratio is 1.0 on the basis of EDX analysis (Fig. S2, ESI†). Supported AgI particles can be obtained via the anion exchange between AgVO₃ and KI. The as-prepared AgI/AgVO₃ composites contain Ag, V, O, and I elements (Fig. S2, ESI†) and the atom content of I increases with increasing KI concentration in the preparation process. This is in agreement with the XRD results and SEM images. Furthermore, based on the EDX results in Table 1, it can be concluded that the atom ratio of Ag to the sum of V and I is approximately 1.0, suggesting that no Ag⁰ particles exist in AgI/AgVO₃ composites. Additionally, as indicated in Table 1,

the specific BET areas of β -AgVO₃ and AgI are limited and the effect of coupling with different quantities of AgI is unobvious.

Table 1 EDX results and specific surface area of pure β -AgVO₃, AgI/AgVO₃ composites, and AgI samples.

Catalyst	Atomic content (at. %)				S_{BET} (m ² ·g ⁻¹)
	Ag	V	I	O	
β -AgVO ₃	16.88	16.84	0	66.28	3.096
5% AgI/AgVO ₃	14.71	14.38	0.30	70.61	3.870
10% AgI/AgVO ₃	15.36	14.59	0.65	69.40	4.682
20% AgI/AgVO ₃	15.74	14.42	1.29	68.55	5.618
30% AgI/AgVO ₃	16.97	14.73	2.34	65.96	7.023
40% AgI/AgVO ₃	18.50	14.88	3.41	63.21	6.309
AgI	50.16	0	49.84	0	1.518

To investigate the optical absorption properties, UV-vis DRS of AgI/AgVO₃ samples, together with that of pure β -AgVO₃ and AgI are depicted in Fig. 4A. As indicated from Fig. 4A, AgI has a clear adsorption edge at around 460 nm, whereas β -AgVO₃ has a broader absorption in the visible region with an absorption edge at about 610 nm. One thing to be noted is that the absorbance intensity displays a moderate enhancement with the increase of AgI contents in the AgI/AgVO₃ composites. The band gap of a semiconductor could be obtained according to the formula: $\alpha h\nu = A (h\nu - E_g)^{n/2}$, where α , $h\nu$, A , and E_g are the absorption coefficient, photo energy, a constant, and band gap, respectively. Among them, the value of n is dependent on the type of semiconductor. As AgI and β -AgVO₃ are direct transition semiconductors,^{23,31} the value of n is 1. Based on the curves of $(\alpha h\nu)^2$ versus $h\nu$ indicated in Fig. 4B, the band gap E_g of AgI and β -AgVO₃ has been deduced to be 2.76 eV and 2.15 eV, respectively. Moreover, the band structure of the as-prepared samples can be determined from the following formula $E_{\text{VB}} = \chi - E^{\circ} + 0.5 E_g$, in which E_{VB} is the potential of valence band edge, χ is the

electronegativity of a semiconductor, and E^c is the energy of free electrons on hydrogen scale with the value of about 4.5 eV. The χ value of β -AgVO₃ and AgI are 5.88 and 5.48 eV. According to the above empirical equation, E_{VB} of β -AgVO₃ and AgI are estimated to be 2.46 and 2.36 eV vs NHE. Based on the equation $E_{CB} = E_{VB} - E_g$, the corresponding E_{CB} are also calculated to be 0.31 and -0.40 eV, respectively.

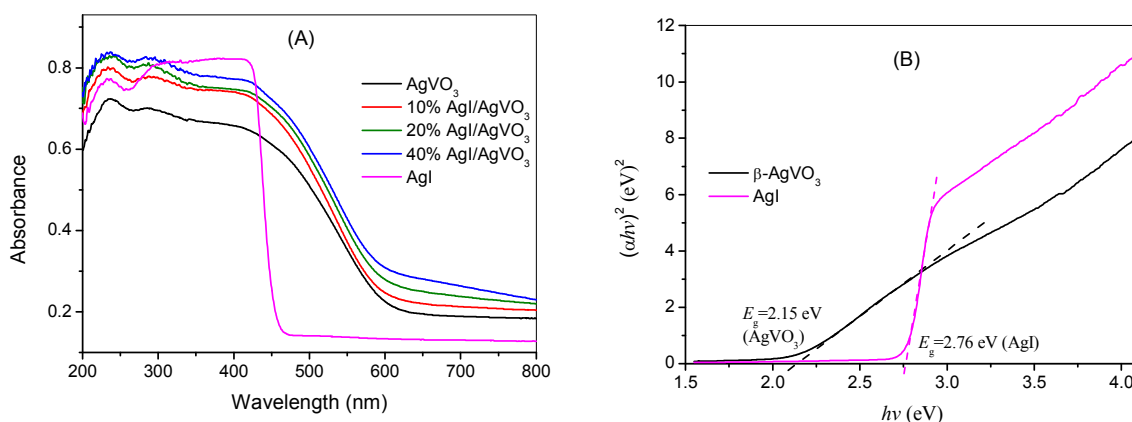


Fig. 4 (A) UV-vis DRS of β -AgVO₃ nanoribbon, 10% AgI/AgVO₃, 20% AgI/AgVO₃, 40% AgI/AgVO₃, and AgI. (B) The plots of $(\alpha h\nu)^2$ versus $h\nu$ of pure β -AgVO₃ and AgI.

3.2 Photocatalytic redox activity of AgI/AgVO₃ composites

The photocatalytic performances of as-obtained samples for the selective oxidation of benzylamine are depicted in Fig. 5. No reactant is converted in the absence of visible light illumination or photocatalysts, confirming the oxidation of benzylamine is proceeded by a photocatalytic mechanism. As indicated in Fig. 5, although pure β -AgVO₃ or AgI can oxidate benzylamine to target product imine, the conversion rate is low. β -AgVO₃ and AgI exhibit limited conversion yield of 10.5 % and 22.4% after 12 h of visible light illumination, respectively. In contrast, the AgI/AgVO₃ composites prepared via in-situ growth approach possess significantly enhanced photocatalytic activities and the as-obtained photocatalysts display good selectivity (> 95%) for the oxidation of benzylamine to product imine. More importantly, it is found the AgI quantities play a vital role in the oxidation properties of as-prepared nanocomposites. The conversion rate of reactant benzylamine increases gradually from bare β -AgVO₃, 5% AgI/AgVO₃, 10% AgI/AgVO₃, to 20% AgI/AgVO₃. However, as the amount of

supported AgI on β -AgVO₃ nanoribbon increases further, the conversion rate of benzylamine declines, suggesting that the excessive AgI is unfavorable for the photocatalytic selective oxidation. The possible reason is that high content of AgI particles with larger size might interfere with the light absorption of active sites. Therefore, the sample 20% AgI/AgVO₃ exhibits the highest activity for benzylamine oxidation and gives a conversion rate of 88.2 % after 12 h irradiation with visible light.

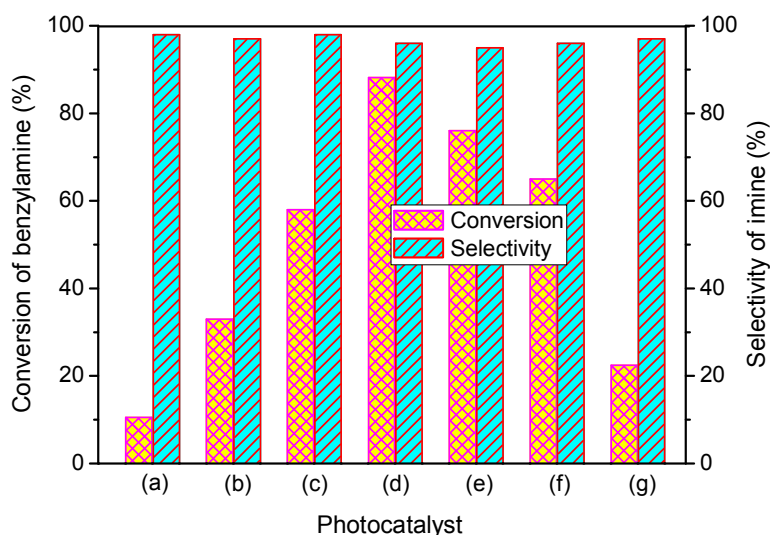


Fig. 5 The selective oxidation of benzylamine over the heterojunction AgI/AgVO₃ nanoribbons under visible light irradiation: pure β -AgVO₃ (a), 5% AgI/AgVO₃ (b), 10% AgI/AgVO₃ (c), 20% AgI/AgVO₃ (d), 30% AgI/AgVO₃ (e), 40% AgI/AgVO₃ (f), and AgI (g).

To expand the utilization range of as-prepared AgI/AgVO₃, the photocatalytic oxidation of various substituted benzylamine with the optimal sample 20% AgI/AgVO₃ has been carried out and the results are summarized in Table 2. The structures of products were confirmed by comparison of the retention times with standard samples and GC-MS analysis (Fig. S3, ESI[†]). The selective oxidations of benzylamines proceed smoothly and form the corresponding imines with high product selectivities for all the derivatives. For example, methyl *o*-, *m*-, *p*-substituted benzylamines can be selectively converted to desired products with similar conversions and selectivities. Additionally, it can be found that the electronic effects associated with electron-donation groups (CH₃- and CH₃O-) and electron withdrawing groups (F- and Cl-) on benzene rings have slight influence on the product selectivity and

conversion rate. The results demonstrate the catalytic oxidation of benzylamine is insensitive to the type of substituents and thus has great tolerance of functional-groups.

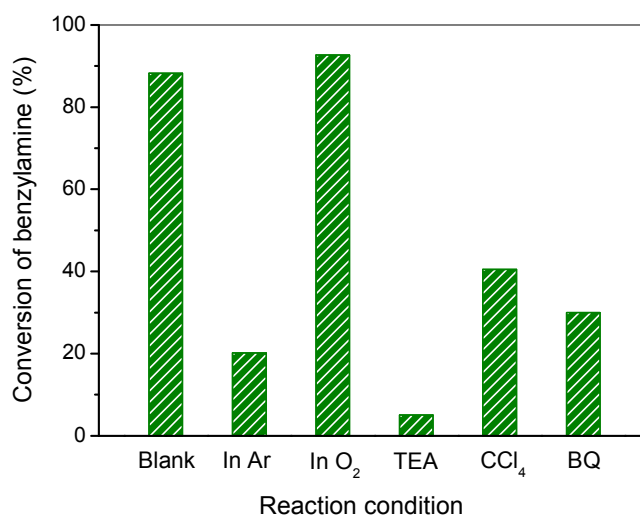
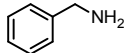
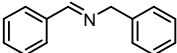
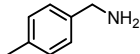
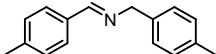
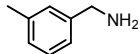
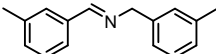
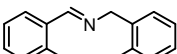
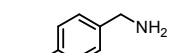
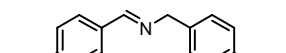
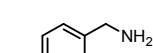
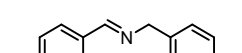
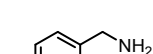
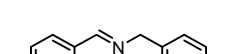


Fig. 6 Controlled experiments using different radical scavenger or reaction atmosphere for the selective conversion of benzylamine to imine over 20% AgI/AgVO₃ photocatalyst.

Additionally, to further study the photocatalytic mechanism of benzylamine oxidation, various controlled experiments by choosing reaction atmosphere or adding radical scavengers are conducted and the results are given in Fig. 6. Firstly, the elimination of air by bubbling with Argon (Ar) results in a low conversion of benzylamine, suggesting dioxygen plays an important role in photocatalytic oxidation of benzylamine. Meanwhile, the conversion of benzylamine in O₂ is 92.7 %, which just slightly increases compared to that in air (88.2 %), which indicates that molecular oxygen in air is adequate for the selective oxidation of benzylamine over 20% AgI/AgVO₃ nanocomposite. When triethanolamine (TEA), a radical scavenger to holes, is added into the reaction system, the conversion of benzylamine decreases dramatically, implying that photoinduced holes (h⁺) are the primary reactive species for the photocatalytic conversion of benzylamine. The additions of tetrachloromethane (CCl₄) for trapping electrons or benzoquinone (BQ) for superoxide radicals (O₂^{•-}), lead to a moderate decrease in the conversion of reactant (Fig. 6). Although photoinduced electrons cannot directly take part in oxidating process, they have the ability to activate molecular oxygen and form O₂^{•-} radicals, which then

participate in the selective conversion of benzylamine. These experimental results indicate explicitly that the photocatalytic oxidation of benzylamine with AgI/AgVO₃ catalyst is mainly performed by the synergistic effect of photo-holes, electrons and O₂^{•-}.

Table 2 Photocatalytic selective conversion of various benzylamine with 20% AgI/AgVO₃ nanocomposite under visible-light irradiation.

Entry	Reactant	Product	Time (h)	Conv. (%)	Sel. (%)
1			12	88.2	96
2			10	86.5	97
3			10	77.3	96
4			10	85.0	95
5			7.5	91.8	95
6			13.5	87.0	94
7			12	85.6	93

Reaction conditions: 20% AgI/AgVO₃ (50 mg), benzylamine (0.25 mmol), acetonitrile (10 mL), in air.

Except for the excellent photocatalytic performance toward the selective oxidation of benzylamine, the nanocomposites of AgI/AgVO₃ also display improved photo-activity for reduction of toxic Cr(VI) in water, which is considered as an effective way to retard Cr(VI) pollutions. Fig. 7 presents the results of photocatalytic reduction Cr(VI) over different AgI/AgVO₃ nanocomposites, together with pure β-AgVO₃ and AgI. In the absence of photocatalysts, no obvious change in Cr(VI) concentrations is observed. As displayed in Fig. 7, AgI/AgVO₃ nanocomposites exhibit significantly improved photo-reduction activity in comparison with pure β-AgVO₃ and bare AgI under visible light illumination for 120 min. Analogous to the results of selective oxidation benzylamine, the loading

content of AgI in the as-obtained AgI/AgVO₃ nanoribbons has an essential effect on the photo-activity for reduction Cr(VI). Among these composites, 20% AgI/AgVO₃ sample displays the highest photo-reduction activity and gives rise to a removal rate of 96.5% after 120 min of visible light irradiation. The low photo-activity over β -AgVO₃ nanoribbon could be attributed to its positive conduction band potential and weak reductive property. Bare AgI sample also shows low photo-reduction ability toward removal of Cr(VI), which might be ascribed to the inhomogenous size and obvious aggregation of AgI particles (Fig. S1, ESI†).

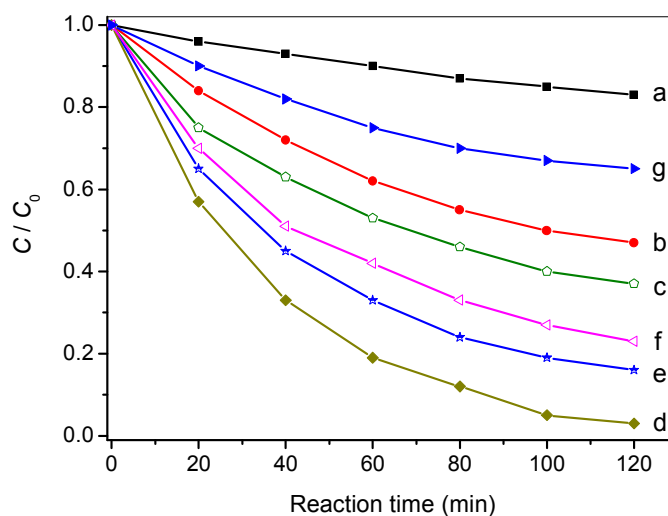


Fig. 7 Photocatalytic reduction of Cr(VI) over AgI/AgVO₃ nanoribbon-like composites under visible light irradiation: β -AgVO₃ (a), 5% AgI/AgVO₃ (b), 10% AgI/AgVO₃ (c), 20% AgI/AgVO₃ (d), 30% AgI/AgVO₃ (e), 40% AgI/AgVO₃ (f), and bare AgI (g).

Additionally, controlled experiment by adding K₂S₂O₈ (a trapping agent of photoinduced electrons, 0.1 mmol)³³ into the present system is carried out and the corresponding result is presented in Fig. S4, ESI†. It can be seen clearly that photocatalytic reduction Cr(VI) over the typical catalyst of 20% AgI/AgVO₃ hardly occurs, which demonstrates the photo-reduction of Cr(VI) is conducted by photoinduced electrons under visible light illumination. The results of redox reactions indicate that AgI/AgVO₃ nanocomposites prepared via in-situ growth approach can serve as potential visible-light-driven photocatalysts. The 20% AgI/AgVO₃ sample, which exhibits the optimal

photo-activity toward selective oxidation of benzylamine and reduction of Cr(VI) ions, is selected for the following mechanism study.

3.3 Improved photocatalytic mechanism of AgI/AgVO₃ nanocomposites

The results of controlled experiments by adding different trapping agents, shown in Fig. 6 and Fig. S4, indicate that the selective oxidation of benzylamine is driven by photogenerated holes and the photo-reduction of toxic Cr(VI) is performed by photogenerated electrons over as-prepared AgI/AgVO₃ nanocomposites with visible light. The remarkably enhanced photocatalytic performance of AgI/AgVO₃ samples, compared with bare AgVO₃ and AgI, could be ascribed to the efficient separation of photogenerated charge carriers via the formation of ribbon-like heterostructures between β -AgVO₃ and AgI. In general, the photoluminescence emission spectra (PLs) are considered as an effective technology to investigate the transfer and fate of photoinduced carriers.^{33,34} The higher PL intensity represents the less separation capacity of photoinduced charge carriers and the lower photocatalytic activity in semiconductor-based system. Fig. 8A depicts the PL spectra of β -AgVO₃, 20% AgI/AgVO₃, and AgI with an excitation wavelength of 400 nm. It can be observed that pure β -AgVO₃ exhibits a strong emission peak at about 480 nm and a shoulder peak around 580 nm. The high intensity of AgVO₃ emissive spectrum suggests the electrons and holes over β -AgVO₃ nanoribbons are facile to recombine. Meanwhile, the emission spectrum of bare AgI also displays relatively high intensity and is centered at 470 nm, corresponding to the intrinsic luminescence of AgI.³⁰ However, for the 20% AgI/AgVO₃ sample, the relative low PL intensity implies that photogenerated electrons and holes can migrate effectively between AgVO₃ and AgI and thus inhibit the recombination of charge carriers.

Transient photocurrent measurements are also performed to evaluate the separation capacity of photoinduced carriers and the results are presented in Fig. 8B. The AgI/AgVO₃ composites exhibit dramatically improved photocurrent responses in comparison with blank AgVO₃ and AgI. As shown in Fig. 8B, 20% AgI/AgVO₃ sample shows a significantly improved photocurrent density of 0.41 $\mu\text{A}\cdot\text{cm}^{-2}$, which is about 4 times of β -AgVO₃ and 2 times of AgI. The results of transient photocurrent are coincident with those of PL spectra, which indicate more effective separation and migration of

photoinduced electrons and holes over AgI/AgVO₃ nanocomposites.

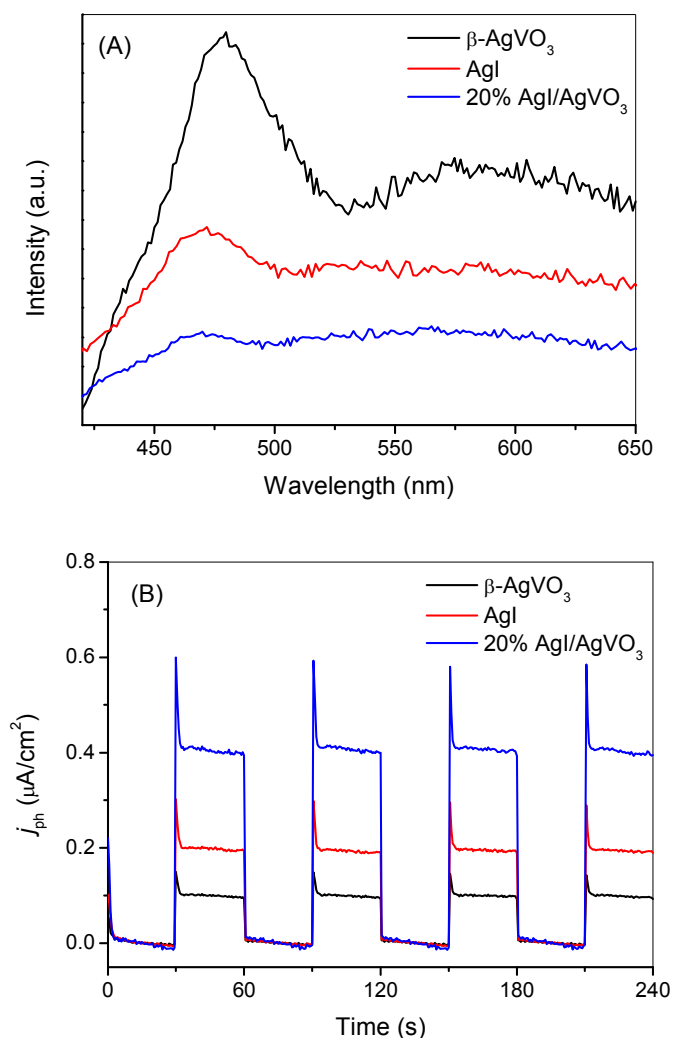


Fig. 8 (A) Photoluminescence spectra with an excitation wavelength at 400 nm and (B) Transient photocurrent response of bare β -AgVO₃, 20% AgI/AgVO₃ nanocomposite, and pure AgI.

Most of the heterostructure nanocomposites have followed a bidirectional charge transfer mechanism.³⁵⁻³⁷ For example, Kumar have reported that the photoinduced electrons enrich on the conduction-band of Ag₃PO₄ and holes on the valence-band of g-C₃N₄, which are conducted by a double charge transfer process between Ag₃PO₄ and g-C₃N₄.³⁵ As for the as-prepared AgI/AgVO₃ nanocomposites, the following charge migration procedure should occur, supposing the above-mentioned bidirectional charge transfer is the primary migration process. Photogenerated

electrons can be transferred from the E_{CB} of AgI into that of β -AgVO₃ and meantime photogenerated holes from the E_{VB} of β -AgVO₃ into that of AgI, based on the relative position of E_{VB} or E_{CB} of AgI and β -AgVO₃ obtained from Fig. 4. As a result, photo-electrons enrich on E_{CB} of AgVO₃ and photo-holes on E_{VB} of AgI in the nanocomposites AgI/AgVO₃. The low E_{CB} of AgVO₃ (0.31 eV vs NHE) demonstrates that the photo-electrons cannot reduce dioxygen to generate superoxide anionic radicals because the redox potential for O₂/O₂^{•-} is -0.16 V vs NHE.³⁸ However, it can be clearly observed from Fig. 9 the characteristic signals for the adduct DMPO-O₂^{•-} formed^{39,40} over AgI/AgVO₃ composites and bare AgI in methanol solution under the irradiation of visible light, whereas no corresponding signals are obtained with pure β -AgVO₃. It demonstrates that photo-electrons located on E_{CB} of AgI can reduce O₂ to O₂^{•-} while those on E_{CB} of β -AgVO₃ cannot. On the other hand, the strong signals of DMPO-O₂^{•-} obtained over 20% AgI/AgVO₃ nanocomposites explicitly indicate that the above-mentioned double charge transfer cannot be the main migration process of photoinduced carriers in the present AgI/AgVO₃ composites.

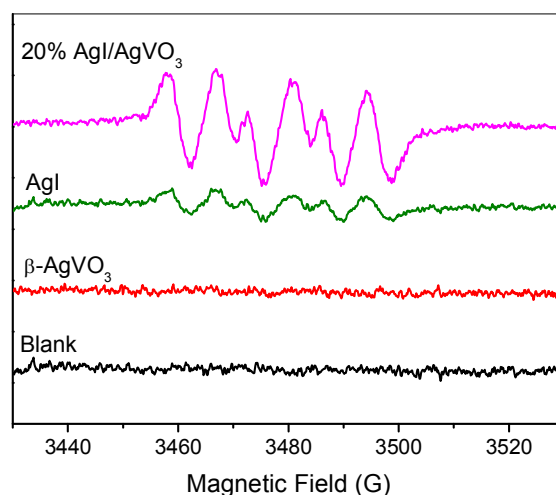


Fig. 9 DMPO spin-trapping ESR spectra recorded after 5 min of visible light irradiation in methanol dispersion of bare β -AgVO₃, 20% AgI/AgVO₃ nanocomposite, and pure AgI. The blank represents the sample containing spin probe alone under light illumination, and the sample containing spin probe and catalysts in dark.

To further clarify the improved charge transfer mechanism of AgI/AgVO₃ hybrid photocatalysts, the used sample of 20% AgI/AgVO₃ are analyzed by using XPS and the corresponding results are presented in Fig. 10. The survey XPS spectra display the sample consists of Ag, I, O, and V elements (Fig. 10A). Two peaks at 516.9 and 524.5 eV can be assigned to V 2p_{5/2} and V 2p_{3/2} of V⁵⁺ in the β-AgVO₃.^{20,41,42} The peaks at 619.9 and 631.4 eV should originate from I 3d of AgI.⁴³ As shown in Fig. 10B, the Ag 3d peaks of used AgI/AgVO₃ can be fitted and separated into two set of XPS peaks by using XPSPEAK software. The strong peaks at 368.2 and 374.3 eV belong to Ag⁺ in β-AgVO₃ and AgI,^{20,43} whereas the weak peaks at 368.5 and 374.6 eV are ascribed to Ag⁰ species.³¹

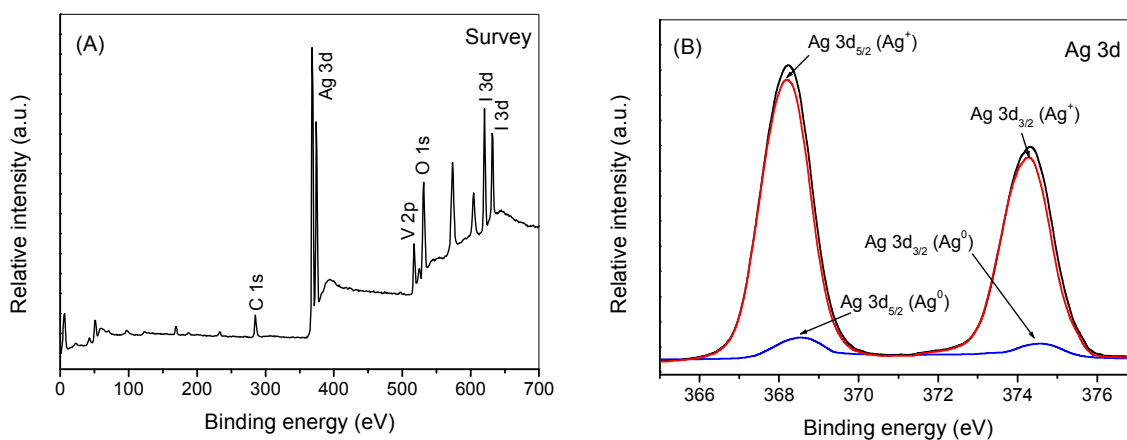


Fig. 10 Survey XPS spectra (A) and high resolution XPS spectra of Ag 3d (B) over 20% AgI/AgVO₃ sample after used for 1 recycling run.

In general, silver halides (AgX) are facile to decomposing into Ag⁰ under light irradiation owing to the strong photosensitization property, especially for AgCl and AgBr materials. However, the studies have indicated that supported AgX possess higher photostability and photocatalytic performance toward pollutants degradation and disinfection.^{30,44,45} For the as-synthesized AgI/AgVO₃ nanocomposites, a small amount of Ag⁰ is formed on the surface of photocatalyst during the selective oxidation of benzylamine, which has been verified by XPS results (Fig. 10B). Whereas, as depicted in Fig. 11, the presence of Ag⁰ has slight influence on the light absorption property of 20% AgI/AgVO₃ sample in the visible range, possibly because of low content of Ag⁰ species. Furthermore, it could be

found from Fig. 11 the photocatalysts after 1.5 h, 1 and 4 recycling runs display almost the same absorption, which suggests that the formed Ag/AgI/AgVO₃ in the initial stage of photocatalytic reaction possess excellent photostability. The EDX results of photocatalyst 20% AgI/AgVO₃ before and after 1.5 h, 1 and 4 recycling runs are also summarized in Table S1, ESI†. The atom contents of formed metallic Ag⁰ are calculated by subtracting the sum of the atom content of V and I from that of Ag. The obtained contents of Ag⁰ do not have evident changes over 20% AgI/AgVO₃ catalyst used for different reaction time. Besides, as shown in Fig. S5 (ESI†), no obvious decline in reactant conversion and product selectivity is observed after four cycling runs. These results clearly indicate the present AgI/AgVO₃ photocatalysts exhibit good stability and can be reused without regeneration.

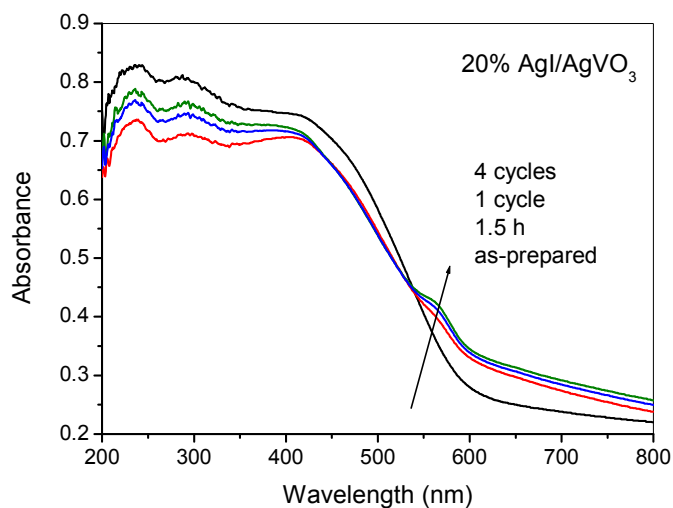
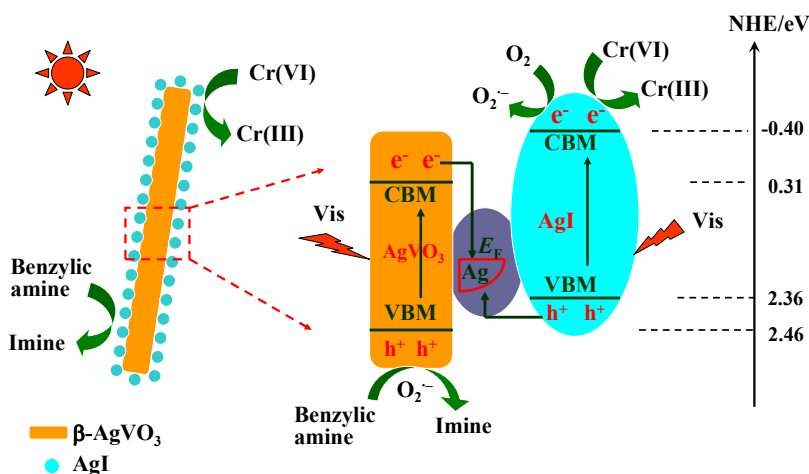


Fig. 11 UV-vis DRS of 20% AgI/AgVO₃ photocatalyst after different reaction time.

In the Ag-based photocatalytic system, the roles of metallic Ag⁰ on enhancing the separation of photoinduced carriers and photocatalytic performance are mainly surface plasmon resonance (SPR) and Z-scheme bridge mechanism. SPR is the resonant photo-induced collective oscillation of surface electrons over Ag nanoparticles and the phenomenon can occur only when the samples exhibit strong light absorption in the SPR band.^{46,47} However, based on the results of Fig. 11, no evident enhancement in light absorption over used AgI/AgVO₃ photocatalyst is observed, compared with as-synthesized sample, which implies that SPR absorption deriving from Ag nanoparticles is weak. Therefore, the SPR effect might not be main role of Ag⁰ in the selective redox reactions with AgI/AgVO₃ heterostructure

photocatalysts.

On the other hand, the formed Ag^0 species in photocatalytic reactions can connect with $\beta\text{-AgVO}_3$ and AgI and serve as a charge migration bridge to drive the efficient separation of photoinduced carriers. Moreover, the above-referred improved photocatalytic redox capacities, the results of radicals trapping experiments, and the formation of superoxide radicals can be explained reasonably using the proposed Z-scheme bridge mechanism. Scheme I displays the possible enhanced mechanism over AgI/ AgVO_3 heterostructure catalysts for the photocatalytic redox reactions. Under visible light illumination, both $\beta\text{-AgVO}_3$ and AgI are photo-excited and holes or electrons are generated on their corresponding valence and conduction band. The electrons on the conduction band of $\beta\text{-AgVO}_3$ facilitate transfer into Ag nanoparticles because the conduction band edge is more negative than the Fermi level of formed Ag^0 . Meanwhile, the holes on the valence band of AgI easily shift into metal Ag^0 , since the valence band of AgI is more positive than Fermi level of metallic Ag. The synergistic charge transfer processes remarkably enhance the separation of photogenerated electrons/holes on the surface of individual AgVO_3 and AgI. Therefore, photo-electrons enrich on the conduction-band of AgI with more negative potential and holes on the valence-band of AgVO_3 with more positive potential, which finally results in the significantly improved photocatalytic performance for redox reactions.



Scheme I Photocatalytic mechanism of AgI/ AgVO_3 toward the selective oxidation of benzylic amine and reduction of Cr(VI) under visible light irradiation.

4. Conclusions

In this study, AgI/AgVO₃ nanoribbon composites have been successfully fabricated via facile in-situ ion exchange between KI and β -AgVO₃. β -AgVO₃ nanoribbons serve as not only Ag sources, but also excellent support to immobilize AgI nanoparticles. The as-synthesized AgI/AgVO₃ nanocomposites possess significantly improved photocatalytic activity in comparison with pure β -AgVO₃ and AgI, toward the selective oxidation of benzylamine and reduction of Cr(VI) under visible light illumination. It is found that the amounts of supported AgI play an important role in the photocatalytic redox activity and 20% AgI/AgVO₃ sample displays the highest photocatalytic performance. Moreover, the formed Ag⁰ species in the initial stage of photocatalytic reaction can serve as a charge migration bridge in the heterostructure catalysts. The superior photocatalytic redox performance is ascribed to the enhanced separation of photoinduced electrons/holes via the Z-scheme bridge mechanism of formed Ag/AgI/AgVO₃.

Acknowledgements

This work was supported by the National Natural Science Foundation of China (21307027, 51074067) and the Foundation of Henan Educational Committee (2010B150009).

Notes and references

^a *Institute of Applied Chemistry, Henan Polytechnic University, Jiaozuo, 454003, P.R. China*

Fax: +86-391-3987811; Tel: +86-391-3987818;

E-mail: yangjuanhpu@yahoo.com

^b *State Key Laboratory Cultivation Base for Gas Geology and Gas Control, School of Safety Science and Engineering, Henan Polytechnic University, Jiaozuo, 454003, P.R. China*

† Electronic Supplementary Information (ESI) available: [SEM photograph of pure AgI; EDX patterns of β -AgVO₃ and 30% AgI/AgVO₃ nanocomposite; GC and GC-MS data for representative compounds in Table 2; controlled experiment of photo-reduction Cr(VI) over 20% AgI/AgVO₃

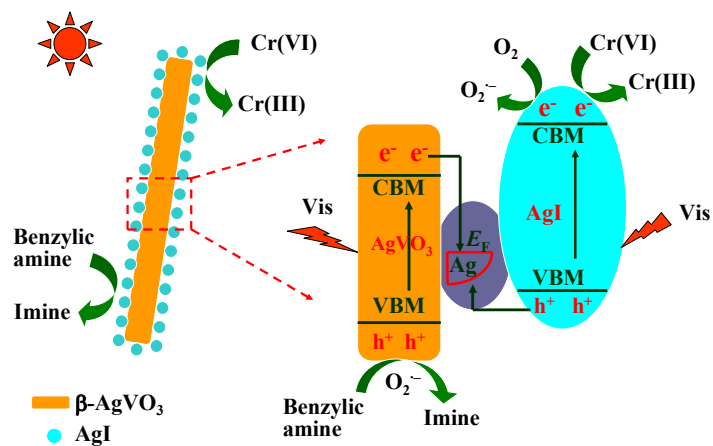
catalyst; EDX results of used 20% AgI/AgVO₃; and cycling experiments toward selective oxidation of benzylamine]. See DOI: 10.1039/x0xx00000x

- 1 M. A. Fox and M. T. Dulay, *Chem. Rev.*, 1993, **93**, 341-357.
- 2 M. R. Hoffmann, S. T. Martin, W. Choi and D. W. Bahnemann, *Chem. Rev.*, 1995, **95**, 69-96.
- 3 A. Mills and S. Le Hunte, *J. Photochem. Photobiol., A*, 1997, **108**, 1-35.
- 4 A. L. Linsebigler, G. Lu and J. T. Yates, *Chem. Rev.*, 1995, **95**, 735-758.
- 5 A. Fujishima, T. N. Rao and D. A. Tryk, *J. Photochem. Photobiol., C*, 2000, **1**, 1-21.
- 6 R. Daghrir, P. Drogui and D. Robert, *Ind. Eng. Chem. Res.*, 2013, **52**, 3581-3599.
- 7 Z. G. Yi, J. H. Ye, N. Kikugawa, T. Kako, S. X. Ouyang, H. Stuart-Williams, H. Yang, J. Y. Cao, W. J. Luo, Z. S. Li, Y. Liu and R. L. Withers, *Nat. Mater.*, 2010, **9**, 559-564.
- 8 Y. Bi, S. Ouyang, N. Umezawa, J. Cao and J. Ye, *J. Am. Chem. Soc.*, 2011, **133**, 6490-6492.
- 9 J. Wang, F. Teng, M. Chen, J. Xu, Y. Song and X. Zhou, *CrystEngComm*, 2013, **15**, 39-42.
- 10 P. Wang, B. B. Huang, X. Y. Qin, X. Y. Zhang, Y. Dai, J. Y. Wei and M. H. Whangbo, *Angew. Chem., Int. Ed.*, 2008, **47**, 7931-7933.
- 11 M. S. Zhu, P. L. Chen and M. H. Liu, *ACS Nano*, 2010, **5**, 4529-4536.
- 12 C. W. Xu, Y. Y. Liu, B. B. Huang, H. Li, X. Y. Qin, X. Y. Zhang and Y. Dai, *Appl. Surf. Sci.*, 2011, **257**, 8732-8736.
- 13 G. P. Dai, J. G. Yu and G. Liu, *J. Phys. Chem. C*, 2012, **116**, 15519-15524.
- 14 F. Y. Cheng and J. Chen, *J. Mater. Chem.*, 2011, **21**, 9841-9848.
- 15 J. Ren, W. Z. Wang, M. Shang, S. M. Sun, L. Zhang and J. Chang, *J. Hazard. Mater.*, 2010, **183**, 950-953.
- 16 L. Q. Mai, L. Xu, Q. Gao, C. H. Han, B. Hu and Y. Q. Pi, *Nano Lett.*, 2010, **10**, 2604-2608.
- 17 H. Xu, H. M. Li, L. Xu, C. D. Wu, G. S. Sun, Y. G. Xu and J. Y. Chu, *Ind. Eng. Chem. Res.*, 2009, **48**, 10771-10778.
- 18 H. F. Shi, Z. S. Li, J. H. Kou, J. H. Ye and Z. G. Zou, *J. Phys. Chem. C*, 2011, **115**, 145-151.

- 19 P. Ju, H. Fan, B. L. Zhang, K. Shang, T. Liu, S. Y. Ai and D. Zhang, *Sep. Purif. Technol.*, 2013, **109**, 107-110.
- 20 Y. Sang, L. Kuai, C. Y. Chen, Z. Fang and B. Y. Geng, *ACS Appl. Mater. Interfaces*, 2014, **6**, 5061-5068.
- 21 W. Zhao, Y. Guo, Y. Faiz, W. T. Yuan, Cheng. Sun, S. M. Wang, Y. H. Deng, Y. Zhuang, Y. Li, X. M. Wang, H. He and S. G. Yang, *Appl. Catal. B: Environ.*, 2015, **163**, 288-297.
- 22 W. Zhao, F. Liang, Z. M. Jin, X. B. Shi, P. H. Yin, X. R. Wang, C. Sun, Z. Q. Gao and L. S. Liao, *J. Mater. Chem. A*, 2014, **2**, 13226-13231.
- 23 Y. M. Yang, Y. Y. Liu, B. B. Huang, R. Zhang, Y. Dai, X. Y. Qin and X. Y. Zhang, *RSC Adv.*, 2014, **4**, 20058-20061.
- 24 C. Hu, T. W. Peng, X. X. Hu, Y. L. Nie, X. F. Zhou, J. H. Qu and H. He, *J. Am. Chem. Soc.*, 2010, **132**, 857-862.
- 25 J. L. Wang, Y. Yu and L. Z. Zhang, *Appl. Catal. B: Environ.*, 2013, **136**, 112-121.
- 26 S. C. Yan, Z. S. Li and Z. G. Zou, *Langmuir*, 2010, **26**, 3894-3901.
- 27 X. C. Wang, K. Maeda, A. Thomas, K. Takanabe, G. Xin, J. M. Carlsson, K. Domen and M. Antonietti, *Nat. Mater.*, 2009, **8**, 76-80.
- 28 J. E. Chateauneuf, *J. Am. Chem. Soc.*, 1990, **112**, 442-444.
- 29 J. Yang, X. H. Wang, Y. M. Chen, J. Dai and S. H. Sun, *RSC Adv.*, 2015, **5**, 9771-9782.
- 30 H. F. Cheng, B. B. Huang, Y. Dai, X. Y. Qin and X. Y. Zhang, *Langmuir*, 2010, **26**, 6618-6624.
- 31 Z. H. Chen, W. L. Wang, Z. G. Zhang and X. M. Fang, *J. Phys. Chem. C*, 2013, **117**, 19346-19352.
- 32 J. H. Yi, L. L. Huang, H. J. Wang, H. Yu and F. Peng, *J. Hazard. Mater.*, 2015, **284**, 207-214.
- 33 S. Q. Liu, M. Q. Yang, Z. R. Tang and Y. J. Xu, *Nanoscale*, 2014, **6**, 7193-7198.
- 34 N. Wu, J. Wang, D. N. Tafen, H. Wang, J.-G. Zheng, J. P. Lewis, X. Liu, S. S. Leonard and A. Manivannan, *J. Am. Chem. Soc.*, 2010, **132**, 6679-6685.
- 35 S. Kumar, T. Surendar, A. Baruah and V. Shanker, *J. Mater. Chem. A*, 2013, **1**, 5333-5340.
- 36 P. Xiong, J. W. Zhu and X. Wang, *Ind. Eng. Chem. Res.*, 2013, **52**, 17126-17133.
- 37 Y. M. Lin, D. Z. Li, J. H. Hu, G. C. Xiao, J. X. Wang, W. J. Li and X. Z. Fu, *J. Phys. Chem.*

- C*, 2012, **116**, 5764-5772.
- 38 P. M. Wood, *Biochem. J.*, 1988, **253**, 287-289.
- 39 J. Yang, C. C. Chen, H. W. Ji and J. C. Zhao, *J. Phys. Chem. B*, 2005, **109**, 21900-21907.
- 40 W. Zhao, C. C. Chen, X. Z. Li, J. C. Zhao, H. Hidaka and N. Serpone, *J. Phys. Chem. B*, 2002, **106**, 5022-5028.
- 41 L. Z. Dong, Y. M. He, T. T. Li, J. Cai, W. D. Hu, S. S. Wang, H. J. Lin, M. F. Luo, X. D. Yi, L. H. Zhao, W. Z. Weng and H. L. Wan, *Appl. Catal. A: Gen.*, 2014, **472**, 143-151.
- 42 Q. Zhu, W. S. Wang, L. Lin, G. Q. Gao, H. L. Guo, H. Du and A. W. Xu, *J. Phys. Chem. C*, 2013, **117**, 5894-5900.
- 43 H. Xu, J. Yan, Y. G. Xu, Y. H. Song, H. M. Li, J. X. Xia, C. J. Huang and H. L. Wan, *Appl. Catal. B: Environ.*, 2013, **129**, 182-193.
- 44 X. X. Hu, C. Hu, T. W. Peng, X. F. Zhou and J. H. Qu, *Environ. Sci. Technol.*, 2010, **44**, 7058-7062.
- 45 C. Hu, X. X. Hu, L. S. Wang, J. H. Qu and A. M. Wang, *Environ. Sci. Technol.*, 2006, **40**, 7903-7907.
- 46 R. Jin, Y. C. Cao, C. A. Mirkin, K. L. Kelly, G. C. Schatz and J. G. Zheng, *Science*, 2001, **294**, 1901-1903.
- 47 S. Link and M. A. El-Sayed, *J. Phys. Chem. B*, 1999, **103**, 8410-8426.

Graphical Abstract



The improved photocatalytic redox activity over AgI/AgVO₃ nanocomposites is ascribed to efficient separation of photoinduced electrons/holes via Z-scheme bridge mechanism.